Simulations of Non-resolved, Infrared Imaging of Satellites

Kevin T.C. Jim, Basil Scott, Russell Knox

Oceanit, 828 Fort St. Mall, Suite 600, Honolulu, HI 96816

kjim@oceanit.com

ABSTRACT

To determine the feasibility of observing geosynchronous satellites during the daytime, we create a radiometric simulation of a geostationary satellite, coupled with a radiative transfer simulation of the atmosphere, in order to predict the signal-to-noise ratio of such satellites as viewed from a telescope. We find that the observation of GEO satellites is possible, given the right circumstances.

Subject headings: SNR, signal-to-noise ratio, infrared, satellite, MODTRAN, atmospheric simulation

1. Introduction

The geostationary earth orbit (GEO) belt is of great importance because of the large number of vital communications and Earth-observation satellites there. At 36,000 km above the Earths equator, the orbital velocity of satellites in circular orbits matches the speed of the rotation of the Earth. Within the GEO regime, there are geostationary satellites, which maintain their position over a location on the earth, other satellites with orbits that are inclined with respect to the equator, as well as other satellites that do not actively maintain their position or are in slightly different orbits (disposal orbits) and thus move slowly relative to the earths surface. GEO objects are subject to perturbations caused by a number of effects that can cause satellites to drift from a stationary position. Monitoring of the satellites in the GEO belt is necessary to maintain knowledge of their orbits to avoid collisions, to understand whether the satellites are maintained under operator control or if they are out of control, to help to determine why a satellite that fails might have failed, and to determine what is wrong with satellites that are having control problems in order to regain proper operations.

Ground-based monitoring techniques employ radar and optical telescopes for nighttime observations. To our knowledge, there are no operational ground-based infrared (IR) optical sensors for daylight GEO observation. Many daylight IR experiments and capability tests have been performed, and adressed low earth orbit (LEO) objects, with limiting magnitudes of 7 to 8 in H-band (for example, see [2].) However, observing the median of GEO objects requires an observing limit somewhere between magnitudes 11 to 13.5 in K-band. Magnitude 12.5 corresponds to the median brightness of correlated GEO objects in a European Space Agency survey of the GEO belt median in visual wavelengths [5]. Due to the enhanced reflectivity of solar cells in the infrared and the Vega-induced magnitude zeropoint shift in the IR, we would expect the magnitudes of active GEO objects to be brighter in the near IR than in V-band. That is also shown in our simulations. We recently learned of the spectrophotmetric observations of GEO objects by Skinner et al [8] and the broadband magnitudes of the satellites they observed could be calculated from this data.

2. Atmospheric Simulation

The MODerate resolution atmospheric TRANsmission code (MODTRAN) is an advanced radiative transfer simulation of the Earth's atmosphere [1]. It models the atmosphere as thirty layers, each with different physical character-

istics. MODTRAN incorporates measured and modeled spectra of all of the dominant molecular and ionic components of the atmosphere, and can model multiple scattering from particles. It is useful from the ultraviolet well into the thermal infrared wavelengths. MODTRAN models the atmosphere to 100 km.

For this simulation, we chose to use a Mid-latitude Summer Atmosphere model, with low velocity winds of 4.1 m/s (the average at Mauna Kea.) While Mauna Kea is located in the tropics, our discussions with one of the authors of MODTRAN led us to the undestanding that the Tropical Atmosphere model is meant for tropical rainforests, not the rarefied, dry atmosphere of Mauna Kea. The satellite was selected to be due south of Mauna Kea in a geostationary orbit. The time of day was 0800 local time on the 100th day of the year (April 1.) The altitude of the observing site (H1) was 4200 m above sea level, and the altitude of the satellite (H2) was 36,000 km.

The geometry was of an arbitrary slant path, in MODTRAN terminology. MODTRAN was run twice, and generated a transmission curve through the atmospheric path (see Figure 1). The second time, it created a model radiance along the slant path (see Figure 2). This is the sky brightness model.

3. The signal from the satellite

The satellite itself has potentially a very complex signal, due to its geometry for both reflected and emitted light. We simplify this for our model and consider the case of a spherical satellite with diffuse reflectance. Studies have shown that the mean albedo of GEO objects is about 0.18. The sun-satellite-observer angle, or phase angle P, defines the amount of light reflected from the satellite that is observed by the telescope. The fraction of flux incident on the satellite of radius r observed at the telescope from a range R is:

$$\alpha_{\mathrm{diffuse}}(\lambda) = \frac{2}{3} a(\lambda) r^2 \frac{\sin P + (\pi - P)\cos P}{\pi (R+r)^2} \tag{1}$$

where a is the albedo, which is nominally 0.18 for earth-orbiting objects.

If we consider a telescope, the power on the entrance pupil from the object (the satellite) multiplied by the transmission of the optics is the same as the power incident on the focal plane.

$$\Phi_s(\lambda) = \tau_a(\lambda)\tau_o(\lambda)L_s(\lambda)\frac{A_s A_o}{R^2} = \tau_a(\lambda)\tau_o(\lambda)L_s(\lambda)A_o(\lambda)\Omega_{ot} \tag{2}$$

where τ_a is the atmospheric transmission, τ_o is the transmission of the optics, L_s is the radiance from the object, A_s is the cross-sectional area of the object, A_o is the input pupil area of the telescope, and R is the distance to the source from the telescope. Then Ω_{ot} is the solid angle of the source as seen from the telescope.

Since the solid angle subtended by the satellite is

$$\Omega_{ot} = \frac{A_s}{R^2} \tag{3}$$

The radiance to flux relationship is:

$$L_s(\lambda, t) = \frac{F_s(\lambda, t)}{\Omega_{ot}} = \frac{F_s(\lambda, t)R^2}{A_s} \tag{4}$$

Then Equation 2 becomes

$$\Phi_s(\lambda, t) = \tau_a(\lambda)\tau_o(\lambda)F_{\odot}(\lambda)\alpha(\lambda, t)A_o \tag{5}$$

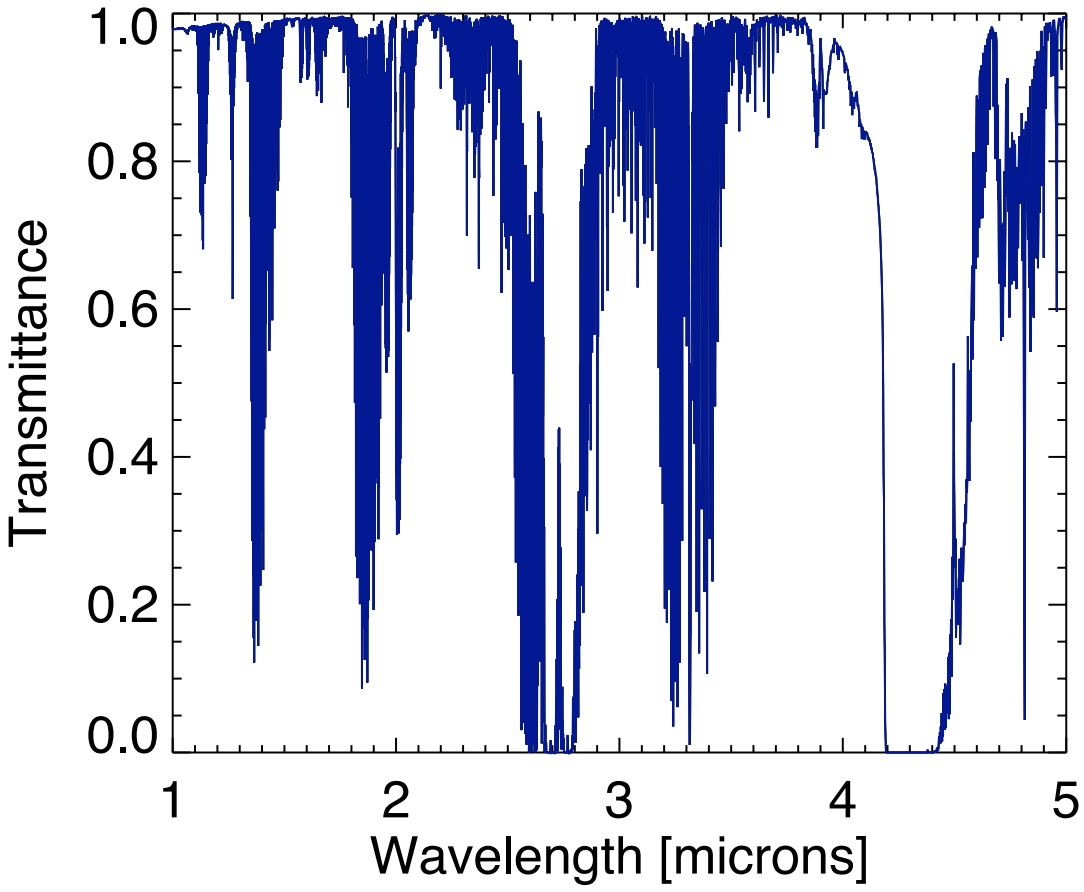

Fig. 1.— The MODTRAN-simulated atmospheric transmission for the Mauna Kea during the day.

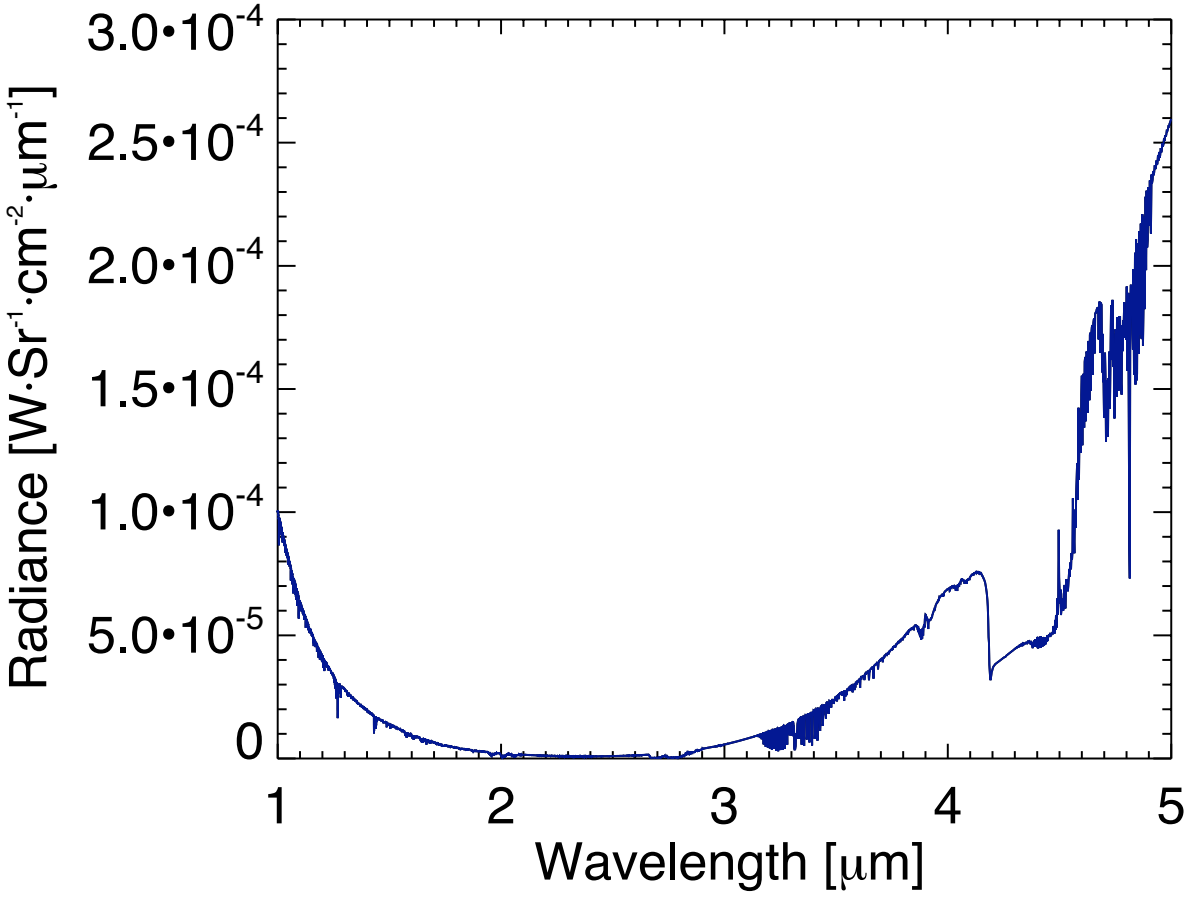

Fig. 2.— The sky radiance along the path to a GEO object south of Mauna Kea in our simulation.

Since the sky is an extended source, and fills the entire field of view, the effective source area is then the entire field of view of the detector. If we consider a pixelated detector, then the individual field of view (IFOV) of one pixel defines the source area, and the power incident on one pixel in the center of the FOV is:

$$\Phi_{sky}(\lambda, t) = \tau_o(\lambda) L_{sky}(\lambda, t) A_d \frac{\pi}{4F^2} \tag{6}$$

where τ_o is the transmission of the optics, L_{sky} is the radiance of the sky, F is the f-number of the system, and A_d is the area of the detector pixel. The sky radiance, L_{sky}, is modeled in MODTRAN.

The power incident on the focal plane is ultimately converted into photo-electrons in the photo-electric types of detectors that we are using. Between 300 nm to 20 um these detectors produce one photo-electron per photon. The satellite signal, assuming that all of the light falls within a single pixel, is:

$$s_s = \int_{\lambda_i}^{\lambda_f} d\lambda \int_{t_i}^{t_f} dt\, \Phi(\lambda, t) \left(\frac{hc}{\lambda}\right)^{-1} q(\lambda) A_d \tag{7}$$

$\left(\frac{hc}{\lambda}\right)^{-1}$ converts from joules to photons and q is the quantum efficiency (photo-electrons counted per incident photon).

For our exposures, which are typically short, we can assume that the change in phase angle over the course of the exposure doesn't change significantly. Likewise, the flux from the Sun should remain about constant over that period of time, leading to the assumption that the radiance from the sky will also change little. Then Equation 7 becomes

$$s_s = \int_{\lambda_i}^{\lambda_f} d\lambda\, \Phi(\lambda) \left(\frac{hc}{\lambda}\right)^{-1} q(\lambda) A_d t \tag{8}$$

t is the exposure time. If we assume that all of the light from the satellite falls into a single pixel, then

$$s_s = \int_{\lambda_i}^{\lambda_f} d\lambda\, \tau_a(\lambda) \tau_o(\lambda) F_{\odot}(\lambda) \alpha(\lambda) A_o \left(\frac{hc}{\lambda}\right)^{-1} q(\lambda) A_d t \tag{9}$$

For the sky background, the signal in a single pixel is:

$$s_{sky} = \int_{\lambda_i}^{\lambda_f} d\lambda\, \tau_o(\lambda) L_{sky}(\lambda) A_d \frac{\pi}{4F^2} \left(\frac{hc}{\lambda}\right)^{-1} q(\lambda) t \tag{10}$$

And the total signal in the pixel is

$$s = s_b + s_s + s_{sky} + t\phi_{dc} \tag{11}$$

ϕ_{dc} is the dark current in electrons per pixel per second, and s_b is the bias constant. Normally, we'll also define

$$s_{dc} = t\phi_{dc} \tag{12}$$

We now examine the noise present in these signals, noting that by convention, the signal-to-noise ratio (SNR) is

$$\mathrm{SNR} = \frac{s_s}{\sigma} \tag{13}$$

σ is usually the single standard deviation noise value. Each of the terms in the single pixel cases has a noise value associated with it. The noise equation for the signal from the satellite is:

$$\sigma^2_{pixel} = s_s + s_{sky} + s_{dc} + \sigma^2_{rn} \tag{14}$$

here σ_{rn} is the read noise of the camera, expressed in electrons. The noise distribution for the other sources are all Poissson, and therefore their uncertainty is the square root of the mean value. This is the simplest form of the noise equation, and is useful for quick approximations. In reality, there are other sources of noise that are typically present.

4. Point Spread Functions and Photometry

Most imaging systems have point spread functions which tend to be larger than a single pixel in extent. Here we refer to the point spread function (PSF) as the convolution of the PSF of the optics and of the distortions caused by the atmosphere. The PSF is highly variable, and is often simply characterized by its full-width at half maximum (FWHM), generally measured in arcseconds.

A commonly used PSF model is based on the Moffat function [6]:

$$I(r) = \frac{\beta - 1}{\pi\alpha^2}\left[1 + \left(\frac{r}{\alpha}\right)\right]^{-\beta} \tag{15}$$

where the full-width at half-maximum (FWHM) is

$$\mathrm{FWHM} = 2\alpha\sqrt{2^{1/\beta} - 1} \tag{16}$$

and

$$I\left(\frac{\mathrm{FWHM}}{2}\right) = \frac{1}{2}I(0) \tag{17}$$

and the total flux is normalized to 1 (Trujillo et al 2001.[12]) We will adopt a working value of $\beta = 2.25$, consistent with the default used in IRAF (Image Reduction Analysis Facility [10].)

We can now solve for α, given FWHM:

$$\alpha = \frac{\mathrm{FWHM}}{2\sqrt{2^{1/\beta} - 1}} \tag{18}$$

The issue with aperture photometry is how to size the aperture so as to optimally capture as much of the source energy as possible without contributing too much to the noise, which is primarily from the background. Irwin et al (2008) find that using an aperture radius equal to the FWHM is the overall best choice, except for the brightest objects. But even for those, they find only a small change in results, on the order of a few mmag ([4].)

So we now have a model to account for variations in seeing that we can extend to any site, knowing in advance what the seeing might be based upon other data. Published data indicate that the intrinsic seeing on Mauna Kea is between 0.25 and 1.2 arcseconds. Most other sites are worse. These are nighttime values; without doubt, the greater heating of the atmosphere will cause worse seeing during the day.

We can now incorporate our simple PSF model into our signal to noise calculations.

The signal S for N samples, each taken with an exposure time of t is:

$$S_N = \sum_N = s_{s,i}t = Ns_st \tag{19}$$

and the variance is

$$\sigma_N^2 = \sum_N \sigma_i^2 = N\left(s_st + n_ps_{\rm sky}t + n_p\sigma_{\rm rn}^2 + n_p * s_{\rm dc}t\right) \tag{20}$$

Then

$$\mathrm{SNR} = \frac{Ns_st}{N^{\frac{1}{2}}}\left(s_st + n_ps_{\rm sky}t + n_p\sigma_{\rm rn}^2 + n_p * s_{\rm dc}t\right)^{-\frac{1}{2}} \tag{21}$$

We desire this SNR to be greater than or equal to a goal SNR_g, so we solve for the number of samples required:

$$N \geq \frac{\mathrm{SNR}_g^2}{s_s^2t^2}\left(s_st + n_ps_{\rm sky}t + n_p\sigma_{\rm rn}^2 + n_p * s_{\rm dc}t\right) \tag{22}$$

5. Telescope and Camera

Through the use of cold stops, the effects of thermal emission are minimized, but not negligible. The telescope we've considered, a 0.5-m RC Optical f/11 telescope, has an obscuration ratio of 0.375 due to the oversized secondary mount. The transmission of the optics, $\tau_o(\lambda)$, is created from a gold-coated, two mirror telescope (approximately 0.95 reflectivity from 1 to 4 microns), convolved with the transmission of IR-optimised relay optics, through a dewar window. We are assuming that the total fractional throughput is 0.57. The self-emission from all of these surfaces amounts to about 11% of the sky background.

Since this is a theoretical exercise, we consider the use of the best of the currently available short wave infrared (SWIR) sensors, such as the Raytheon Virgo array. This device has only 20 electrons of read noise, and is available in several sizes, up to 2048×2048 pixels. The pixels are 20 microns square, and the dark current is negligible if adequately cooled and used for very short exposures. The equivalent Teledyne sensors are also excellent. For a discussion of current infrared technology as applied to astronomy, please refer to Rieke [7]. Assuming that the camera system uses the latest techniques for noise suppression and Fowler sampling, we will assume that the noise will in fact be limited to about 20 electrons for a real camera. There will likely be some additional noise, which we are modeling as an extra 80 electrons. Over this wavelength range, we are assuming a flat quantum efficiency of 0.89.

6. Zeropoint Calibration

The magnitude system is nominally tied to the reference star Vega, which is defined to have a magnitude of 0 in the visible bands, and this is the standard used for many infrared photometric standard star catalogs. AB magnitudes could also be employed, but we will use the Johnson system, in which Vega's magnitude is defined to be 0.0 in each band.

The IRAS satellite discovered that Vega has an excess of infrared emission, greater than what was expected giving a model atmosphere for an A0 star. Subsequent investigation revealed that Vega has an extensive dust disk and is oriented pole-on. Thus Vega may not be the best candidate standard star, but it is well-studied, and it is the most commonly used standard. Absolute spectral calibration standards can be found at the Space Telescope Science Institute website, at http://www.stsci.edu/hst/observatory/cdbs/calspec.html. The Vega calibration is difficult, since the star is too bright to obtain a near infrared spectrum with any of the Hubble Space Telescope instruments. So, for

the near infrared, they employ a model bootstrapped to known spectra in the ultraviolet and visible wavelengths. The units in these files are all in Angstroms and flux given in erg s^{-1} cm^{-2} $Å^{-1}$.

The technique employed is to propagate the spectrum of Vega through the atmosphere at the same location as the satellite, all the way to the focal plane. Using Tokunaga and Vacca's [11] Vega measurements as defining the magnitude standards for each of the near infrared filters, we can then calculate our zeropoint for each filter.

7. Input Data for Modeling

In equations 9 and 10, we listed the terms $\tau_a(\lambda)$, $\tau_o(\lambda)$, $F_\odot(\lambda)$, L_{sky}.

The atmospheric transmission $\tau_a(\lambda)$ is created from MODTRAN models for a specific site, Mauna Kea, at a specific time and slant path to the target. The same simulation is used to find L_{sky}, the sky radiance along the path. Stubbs et al [9] find that the dominant species is water, and so the primary concern is to model that accurately. To that end, we use the same value for the water column as used by Tokunaga and Vacca for Mauna Kea ([11] of 1 mm of precipitable water vapor. The other modeling parameters are from the data are from Erasmus [3].

The solar spectrum, $F_\odot(\lambda)$, is the same one used by MODTRAN - the ASTM E490 solar spectrum, which covers from UV well into the thermal infrared. However, our simulation is integrated over wavelength, so we obtained the spectrum from NASA IPAC, as opposed to using the frequency-domain MODTRAN solar spectrum file.

8. Observational Techniques

Dithering the telescope between exposures allows the more accurate removal of the sky background, which in both daytime and nighttime IR imaging is the dominant source of noise. In addition, dithering prevents the object from landing solely on a bad spot of the detector, and infrared detectors frequently have a higher percentage of defective pixels than CCD's (charge coupled devices) do.

The dithering pattern can be optimized for maximum efficiency by making sure that the steps between the images are a few times the FWHM of the object in the field, but require no more movement of the telescope than necessary. All GEO objects are low SNR objects, because the individual frames must consist of no more than 1 second exposures due to the brightness of the background.

Examination of Figure 2 shows that as the wavelength increases from 1 micron, the sky background drops rapidly to a saddle point, then rises again. The thermal background from warm optics rises, starting a little above 2 microns. So we selected the Kshort filter (1.99 to 2.3 microns) as our candidate pass band for this simulation. It will allow only a small amount of thermal contribution from the telescope, and take advantage of the lower sky emission.

9. Results and Future Work

The simulation showed that, over the wavelengths of the Kshort filter, there is an effective atmospheric transmission of 0.91. The sky background noise was dominant, as expected, with a flux of 34,000 photons per second per pixel. The results are shown in Fig. 3.

We are assuming that the actual SNR results will be worse, but until we obtain data, we cannot say how much worse. The biggest uncertainty is the sky brightness, as it is a simulation result dependent upon a variety of meteoro-

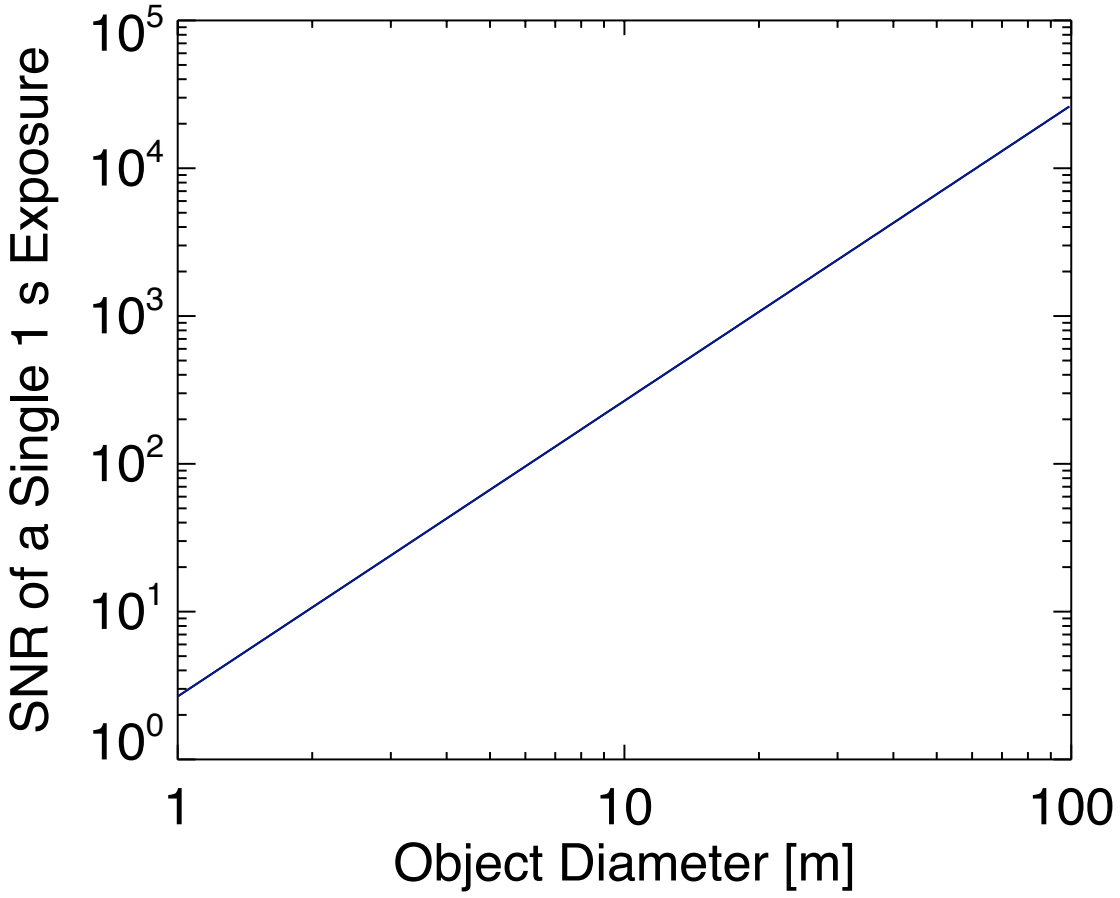

Fig. 3.— The results of the simulation show that under these good circumstances, it is possible to detect a GEO object during the daytime. The site simulated was Mauna Kea with 1 mm of precipitable water vapor, greater than 50 km of visibiity, at 8AM on April 1, looking due South at a geostationary satellite.

logical parameters. In addition, we have not found studies that show the infrared sky brightness during the daytime, except for work done in Antarctica.

In the near future, we will extend this simulation to other sites and parameterize the observatory altitude. We will also examine how the SNR will change with time of day. Finally, we anticipate actual observations will be attempted soon.

REFERENCES

Berk, A., Anderson, G., & Bernstein, L. 1999, Proceedings of SPIE, 3756, 348

Chesser, D. E., Vunck, D., Born, T., Axelson, W., Rehder, K., & Medrano, R. S. 2003, Proc. SPIE, 5082, 1

Erasmus, D. A. 1986, PASP, 98, 254

Irwin, J., Irwin, M., Aigrain, S., Hodgkin, S., Hebb, L., & Moraux, E. 2007, MNRAS, 375, 1449

Jehn, R., Klinkrad, H., Krag, H., Flohrer, T., & Choc, R. 2008, OPS-G Forum, 18 January 2009

Moffat, A. F. J. 1969, Astronomy and Astrophysics, 3, 455, a&AA ID. AAA002.036.009

Rieke, G. H. 2007, Annual Review of Astronomy & Astrophysics, 45, 77

Skinner, M. A., Payne, T. E., Russell, R. W., Guiterrez, D., Crawford, K., Kim, D., Lynch, D. K., Pack, D. W., Rudy, R. J., & Harrington, D. M. 2007, AMOS Proceedings 2007

Stubbs, C. W., High, F. W., George, M. R., DeRose, K. L., Blondin, S., Tonry, J. L., Chambers, K. C., Granett, B. R., Burke, D. L., & Smith, R. C. 2007, The Publications of the Astronomical Society of the Pacific, 119, 1163

Tody, D. 1984, Proc. SPIE, Instrumentation in Astronomy VI

Tokunaga, A. T. & Vacca, W. D. 2005, PASP, 117, 421

Trujillo, I., Aguerri, J. A. L., Cepa, J., & Gutiérrez, C. M. 2001, MNRAS, 328, 977